Feeding *Angptl4*$^{-/-}$ mice *trans* fat promotes foam cell formation in mesenteric lymph nodes without leading to ascites[S]

Antwi-Boasiako Oteng,* Asmita Bhattacharya,† Susanne Brodesser,§ Ling Qi,† Nguan Soon Tan, and Sander Kersten[1,*,††]**

Nutrition, Metabolism, and Genomics Group,* Division of Human Nutrition, Wageningen University, Wageningen, The Netherlands; Division of Metabolism, Endocrinology, and Diabetes,† University of Michigan Medical School, Ann Arbor, MI; Cologne Excellence Cluster on Cellular Stress Responses in Aging-Associated Diseases (CECAD),§ Lipidomics Core Facility, University of Cologne, Cologne, Germany; School of Biological Sciences and Lee Kong Chian School of Medicine,** Nanyang Technological University, Institute of Molecular and Cell Biology, Agency for Science Technology and Research, and KK Research Centre, KK Women's and Children's Hospital, Singapore; and Division of Nutritional Sciences,†† Cornell University, Ithaca, NY

Abstract Angiopoietin-like 4 (ANGPTL4) regulates plasma triglyceride levels by inhibiting LPL. Inactivation of ANGPTL4 decreases plasma triglycerides and reduces the risk of coronary artery disease. Unfortunately, targeting ANGPTL4 for the therapeutic management of dyslipidemia and atherosclerosis is hampered by the observation that mice and monkeys in which ANGPTL4 is inactivated exhibit lipid accumulation in the mesenteric lymph nodes (MLNs). In mice these pathological events exclusively unfold upon feeding a high saturated FA diet and are followed by an ultimately lethal pro-inflammatory response and chylous ascites. Here, we show that *Angptl4*$^{-/-}$ mice fed a diet rich in *trans* FAs develop numerous lipid-filled giant cells in their MLNs, yet do not have elevated serum amyloid and haptoglobin, do not exhibit ascites, and survive, unlike *Angptl4*$^{-/-}$ mice fed a saturated FA-rich diet. In RAW264.7 macrophages, the saturated FA, palmitate, markedly increased markers of inflammation and the unfolded protein response, whereas the *trans*-unsaturated elaidate and the *cis*-unsaturated oleate had the opposite effect. In conclusion, *trans* and saturated FAs have very distinct biological effects in macrophages. Furthermore, lipid accumulation in MLNs is uncoupled from activation of an acute-phase response and chylous ascites, suggesting that ANGPTL4 should not be fully dismissed as target for dyslipidemia.—Oteng, A-B., A. Bhattacharya, S. Brodesser, L. Qi, N. S. Tan, and S. Kersten. **Feeding *Angptl4*$^{-/-}$ mice *trans* fat promotes foam cell formation in mesenteric lymph nodes without leading to ascites. *J. Lipid Res.* 2017.** 58: **1100–1113.**

Supplementary key words atherosclerosis • angiopoietin-like 4 • macrophage foam cells • inflammation • unfolded protein response • lipotoxicity

Elevated plasma levels of LDL-cholesterol are widely accepted to accelerate the development of atherosclerosis. Besides LDL, elevated plasma triglycerides are increasingly recognized as a risk factor for coronary artery disease. More specifically, recent human genetic studies have pointed toward a causal role of hypertriglyceridemia in atherosclerosis development. Accordingly, strategies aimed at reducing hypertriglyceridemia in humans offer a promising therapeutic approach to lower the risk of coronary artery disease. Triglycerides are present in the blood as part of chylomicrons and very low density lipoproteins, and are hydrolyzed by the enzyme, LPL (1). Hence, enhanced hydrolysis of triglycerides by LPL attenuates hypertriglyceridemia and may be targeted to retard the development of coronary artery disease (2).

LPL is produced by a number of cell types, including (cardio)myocytes, adipocytes, and macrophages, and is transported to the luminal surface of capillaries by the protein, glycosylphosphatidylinositol-anchored HDL binding protein 1 (GPIHBP1), which also helps to stabilize LPL (3). Consequently, inactivating mutations in GPIHBP1 give rise to

This work was supported by Nanyang Technological University iFood Research Grant WBS M4081459.080, Fondation Leducq Grant 12CVD04, and by the Graduate School Voeding, Levensmiddelentechnologie, Agro-Biotechnologie en Gezondheid (VLAG) (Wageningen University).

The authors declare that there are no conflicts of interest associated with this manuscript.

Manuscript received 15 December 2016 and in revised form 10 April 2017.

Published, JLR Papers in Press, April 15, 2017
DOI https://doi.org/10.1194/jlr.M074278

Abbreviations: ANGPTL4, angiopoietin-like 4; CLA, conjugated linoleic acid; DMS, dimethylsphingosine; ER, endoplasmic reticulum; GPIHBP1, glycosylphosphatidylinositol-anchored HDL binding protein 1; IRE1, inositol requiring kinase 1; MLN, mesenteric lymph node; PERK, protein kinase RNA-like endoplasmic reticulum kinase; ROS, reactive oxygen species; SAA, serum amyloid A; UPR, unfolded protein response.

[1]To whom correspondence should be addressed.
e-mail: sander.kersten@wur.nl

[S] The online version of this article (available at http://www.jlr.org) contains a supplement.

Copyright © 2017 by the American Society for Biochemistry and Molecular Biology, Inc.

This article is available online at http://www.jlr.org

This is an Open Access article under the CC BY license.

hyperchylomicronemia in mice and humans (4, 5). The activity of LPL is under tight regulation by several proteins to ensure the homeostatic balance in triglyceride disposal under different nutritional and physiological states (6, 7). One of these proteins is angiopoietin-like 4 (ANGPTL4). Following its discovery in 2000 (8, 9), ANGPTL4 has been shown to posttranslationally inhibit LPL activity by promoting the conversion of catalytically active LPL dimers into inactive monomers and by stimulating the intracellular degradation of LPL (10, 11). As a result, overexpression of ANGPTL4 in mice leads to increased plasma triglycerides, whereas the deletion of ANGPTL4 results in lower plasma triglycerides (12, 13). Interestingly, the loss of ANGPTL4 is able to correct the hypertriglyceridemia in *Gpihbp1*$^{-/-}$ mice (14), suggesting that ANGPTL4 may interfere with an accessory transport mechanism for LPL across the endothelium (3). Alternatively, the pronounced lipid lowering caused by loss of ANGPTL4 in *Gpihbp1*$^{-/-}$ mice may be due to enhanced entry of LPL into the bloodstream via the lymph (10).

In humans, carriers of the inactivating E40K mutation in ANGPTL4 have lower plasma triglyceride levels and have a reduced risk of coronary artery disease compared with noncarriers (15, 16). Based on these observations, ANGPTL4 would seem a very attractive pharmacological target to decrease the risk of developing coronary artery disease. However, we and others have shown that inactivating ANGPTL4 in mice fed a diet high in saturated fat elicits severe and ultimately lethal chylous ascites and peritonitis, which is preceded by enlarged mesenteric lymph nodes (MLNs), the presence of lipid-filled giant cells, and a massive acute phase response (17). These effects were coupled to the role of ANGPTL4 as LPL inhibitor in MLN macrophages, thereby preventing excessive FA uptake and a concomitant pro-inflammatory response. The above data have raised serious concerns about the safety of pharmacological targeting of ANGPTL4 in patients. Recently, Dewey et al. (16) reported the accumulation of lipids in MLNs of several female monkeys treated with an anti-ANGPTL4 antibody. However, it is presently unclear whether the accumulation of lipid in MLNs forebodes a marked acute phase response, and is directly connected to the development of chylous ascites and peritonitis. In this context, it is relevant to mention that Dewey et al. (16) did not observe any significant difference between E40K carriers and noncarriers in the rates of diagnosis codes for abdominal lymphatic disorders, as well as ascites, peritonitis, malabsorption, abdominal discomfort, or diarrhea.

Trans FAs are unsaturated FAs that contain one or more double bonds in the *trans* configuration, as opposed to the more common *cis* configuration. *Trans* FAs are synthesized naturally in small amounts in the guts of certain ruminants and are thus contained in meat and dairy products of these animals (18, 19). However, most of the ingested *trans* FAs are synthesized artificially during food processing by partial hydrogenation of vegetable oils to improve the texture and longevity of foods. Numerous epidemiological studies have demonstrated a strong correlation between consumption of industrially produced *trans* FAs and the development of cardiovascular diseases (20–24). Consequently, national policies that either restrict or ban the consumption of *trans* fat-rich foods have been instituted by several countries (25–29).

A *trans* double bond preserves the straight conformation of a FA, whereas a regular *cis* double bond creates a kink in the FA molecule. Because they have a similar linear structure, *trans* FAs are claimed to act like saturated FAs. Indeed, both *trans* and saturated FAs have been shown to raise plasma levels of LDL, which may account for the positive link between *trans* and saturated FA consumption and coronary artery disease (22). However, to what extent *trans* and saturated FAs are interchangeable and share the same cellular effects in vivo and in vitro is not well-known. To further explore this question, we compared the effect of diets rich in *trans* or saturated FAs in *Angptl4*$^{-/-}$ mice, which, as pointed out above, develop a massive acute phase response and ultimately lethal chylous ascites upon feeding a saturated fat-rich diet. These studies were complemented by investigations into the effect of saturated and *trans* FAs in cultured macrophages. Our results indicate that: *a*) *trans* FAs have very distinct effects from saturated FAs in vitro and in vivo; and *b*) the accumulation of lipid in MLNs is uncoupled from the hepatic acute phase response and chylous ascites in *Angptl4*$^{-/-}$ mice fed a diet rich in *trans* FAs.

MATERIALS AND METHODS

Animal treatment

Animal studies were conducted using purebred *Angptl4*$^{-/-}$ mice on a C57Bl/6 background. Male mice 4- to 6-months-old were randomly assigned to three groups (n = 8 per group). Each group was fed a high-fat diet rich in saturated, *cis*-unsaturated, or *trans*-unsaturated FAs for 7 weeks providing 45% energy percent as triglycerides (modified TestDiet 58V8; TestDiet LTD, London), shown in supplemental Table S1. Fat sources were partially hydrogenated soy oil for the *trans* fat diet, canola and palm olein oil for the unsaturated fat diet, and cocoa butter for the saturated fat diet. Bodyweight and food intake were measured weekly. Blood samples were collected at weekly intervals by tail vein bleeding into EDTA-coated tubes. After the dietary intervention, mice were anesthetized with isoflurane, followed by blood collection via orbital puncture. Mice were euthanized by cervical dislocation, after which tissues were excised. Tissues for RNA and protein analysis were immediately frozen in liquid nitrogen and stored at −80°C. Tissues for histological analysis were fixed in 4% paraformaldehyde and later embedded in paraffin. In a second study, nine male *Angptl4*$^{-/-}$ and eight male wild-type mice at 4–6 months of age were placed on the *trans* fat diet for 7 weeks purposely to confirm and to quantify foam cell formation in the MLNs. These animal studies were approved by the Local Animal Ethics Committee at Wageningen University.

FA profiling of test diets by gas chromatography-flame ionization detection

The fat component in the test diets was extracted by the Folch technique, as previously described (30). Briefly, the fats were extracted with a mixture of chloroform and ethanol (2:1 ratio). The addition of water gave a biphasic system, with the fat contained in the chloroform at lower phase. Following purification, the extracted fats were measured gravimetrically. The isolated fats were then saponified with methanolic NaOH and methylated with boron trifluoride to obtain methyl esters. The methyl esters were then fractionated by gas chromatography, detected by flame ionization, and calculated as a fraction of the total amount.

Histology

H&E staining of MLNs was performed using standard protocols. In summary, the MLNs were fixed in 4% paraformaldehyde, processed, and embedded in paraffin blocks. The tissues were then sectioned onto a superfrost glass slide at 3 μm with a microtome. The tissue slices were incubated overnight at 37°C. The slices were stained at room temperature in Mayer hematoxylin solution for 10 min and in eosin Y solution for 10 s. Images were then taken with a light microscope.

Quantification of plasma acute phase proteins, insulin, and glucose

Blood samples were centrifuged at 4°C for 15 min at 10,000 *g*. Plasma was collected and stored at −80°C. ELISA development kits were used to measure plasma serum amyloid A (SAA) (Tridelta Development LTD, Ireland), haptoglobin (Abcam, Cambridge, UK), and lipocalin-2 (Abcam) according to the manufacturer's protocol. Plasma insulin and glucose were measured in plasma samples collected after 2 weeks of dietary intervention, prior to the mice getting visibly ill. Glucose (DiaSys, Germany) and insulin (Crystal Chem, Downers Grove, IL) were measured using dedicated kits.

RNA isolation and quantitative real-time PCR

Total RNA was isolated from mouse liver tissue or cultured RAW264.7 macrophages with TRIzol reagent (Invitrogen, Bleiswijk, The Netherlands) and a Tissuelyser II (Qiagen, Venlo, The Netherlands). Reverse transcription was performed using a First Strand cDNA synthesis kit (Thermo Scientific, Schaumburg, IL) according to the manufacturer's protocol. Quantitative RT-PCR amplifications were performed with iQ SYBR Green Supermix on a CFX384 Touch real-time PCR detection system (Bio-Rad, Hercules, CA). Primer sequences of genes are provided in supplemental Table S2. Expression of target genes was normalized to *36b4*.

Cell culture

Murine RAW264.7 macrophages (ATCC) were cultured in DMEM supplemented with 10% fetal bovine serum, 100 U/ml penicillin, and 1,000 μg/ml streptomycin (Lonza, Verviers, Belgium) in a humidified chamber at 37°C with 5% CO_2.

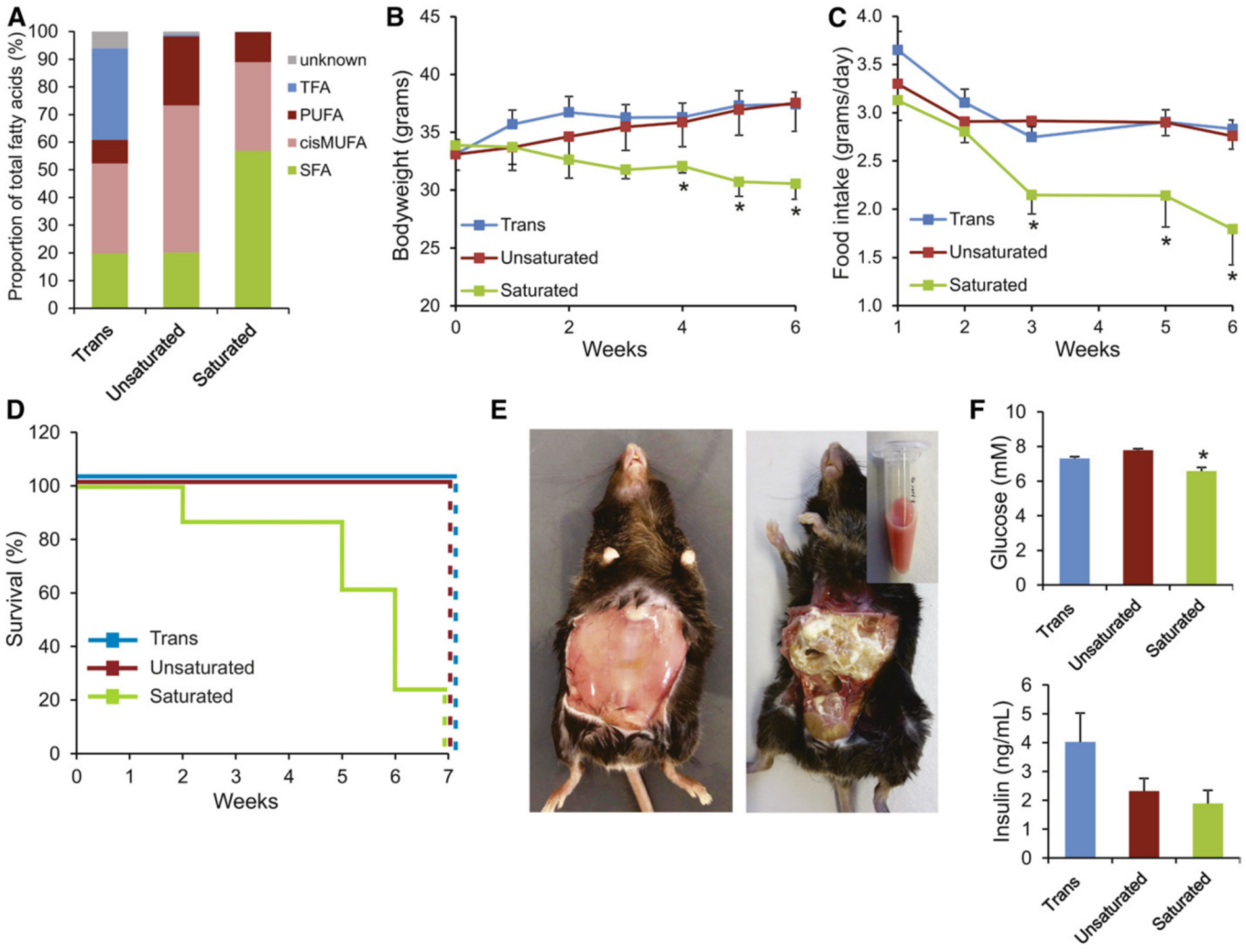


Fig. 1. Feeding *Angptl4*$^{-/-}$ mice a diet rich in saturated, but not *trans*- or *cis*-unsaturated, FAs results in peritonitis, chylous ascites, and death. A: Profile of FA composition in the three test diets. TFA, *trans* unsaturated fatty acids; PUFA, poly-unsaturated fatty acids; cisMUFA, *cis* mono-unsaturated fatty acids; SFA, saturated fatty acids. Changes in body weight (B), average daily food intake (C), and survival (D) of *Angptl4*$^{-/-}$ mice fed the *trans*, unsaturated, or saturated fat diet for 7 weeks. E: Representative pictures of *Angptl4*$^{-/-}$ mice fed the saturated fat diet immediately after euthanization, before (left) and after (right) removal of peritoneum. A sample of the ascites fluid collected from the peritoneum of a single mouse is shown at the top right. F: Plasma levels of glucose and insulin after 2 weeks of feeding. Error bars represent SEM. Asterisk indicates significantly different relative to the *trans* fat group (*$P < 0.05$).

FA preparation and treatment

Palmitate, oleate, and elaidate (Sigma-Aldrich, St. Louis, MO) served as models of saturated, *cis*-unsaturated, and *trans*-unsaturated FAs, respectively. The FAs were reconstituted in ethanol and prepared by dissolving in filter-sterilized 70 mM KOH. The FAs were coupled to FA-free BSA by 30 min incubation at 37°C in prewarmed DMEM containing FA-free BSA. The final working concentration of the FAs was 500 μM and the final ratio of FFA:BSA was 2:1. Vehicle control treatment was prepared using an equivalent mixture of KOH and ethanol. The final concentration of ethanol was less than 0.1%. The RAW264.7 cells were seeded into 6-well plates at 4×10^5 cells per well. After overnight incubation, the cells were incubated with 500 μM of the individual FAs or vehicle control for 6 h. Treatments for experiments were performed in triplicate unless specified otherwise. This procedure was repeated in subsequent experiments with different *trans* FAs [elaidate, *trans*-vaccenate, palmitelaidate, conjugated linoleic acid (CLA) 9Z,11E, and CLA 10E,12Z] and different saturated FAs (laurate, myristate, palmitate, and stearate).

FA treatment of RAW264.7 cells in the presence of chemical inhibitors

Palmitate-treated RAW264.7 cells were cotreated with several chemical inhibitors. Specifically, RAW264.7 cells were treated with 500 μM palmitate for 6 h, and cotreated for the same duration with 10 μM dimethylsphingosine (DMS) (a sphingosine kinase inhibitor), 100 μM sulfosuccinimidyl oleate (CD36 inhibitor), 2.5 μM triascin C (acyl-CoA synthase inhibitor), 50 μM C2-ceramide (membrane-permeable ceramide analog), 10 μM fumonisin B1 (ceramide synthase inhibitor), 10 μM amidepsine A (diglyceride acyltransferase 1 inhibitor), 50 μM etomoxir (carnitine palmitoyl transferase 1 inhibitor), or 10 μM myriocin (serine palmitoyltransferase 1 inhibitor). In a follow-up experiment, RAW 264.7 cells were treated with 500 μM palmitate, oleate, or elaidate for 6 h, and cotreated with 2.5 μM triascin C or 10 μM DMS.

Oil red O staining of lipid droplets

A stock of oil red O was prepared by dissolving 0.5 g in 500 ml of isopropanol. A working concentration was prepared by mixing the stock and ddH_2O at a ratio of 3:2. After treatment, the RAW264.7 cells were washed twice with PBS, fixed with 4% paraformaldehyde for 30 min, and incubated with filtered oil red O dye for 20 min. The cells were then carefully washed three times with ddH_2O. Pictures were taken by light microscope.

Triglyceride quantification

Following treatment, cells were washed twice with PBS. In 6-well plates, 500 uL Tris-EDTA buffer [25 mM Tris, 1 mM EDTA (pH 7.5)] was added to the cells and to prepared triglyceride standards (Instruchemie, The Netherlands). The plates were subsequently put at −80°C for 1 h. The plates were allowed to thaw to room temperature, followed by the addition of 200 μl tertiary butanol and 50 μl methanol. The plates were then shaken at 270 rpm for 15 min and allowed to evaporate on a hot plate at 60°C. Monocolor reagent (Instruchemie) was then added to the wells, followed by shaking for 5 min at 250 rpm on a plate shaker. Samples and standards were transferred to 96-well plates and absorbance was measured at 492 nm. Triglyceride content was normalized to protein content, which was quantified by the Pierce BCA protein assay (Thermo Scientific) according to manufacturer's protocol.

Measurement of oxidative stress

Intracellular reactive oxygen species (ROS) production was measured using DCFDA cellular ROS detection assay kit (Abcam; ab11385) according to manufacturer's protocol. In brief, RAW264.7 cells were seeded into 96-well plates at 2×10^4 cells per well. After overnight incubation, cells were washed with PBS and incubated with 20 μM DCFDA dye for 45 min at 37°C in the dark. The cells were then washed with PBS and incubated for 6 h with FAs or

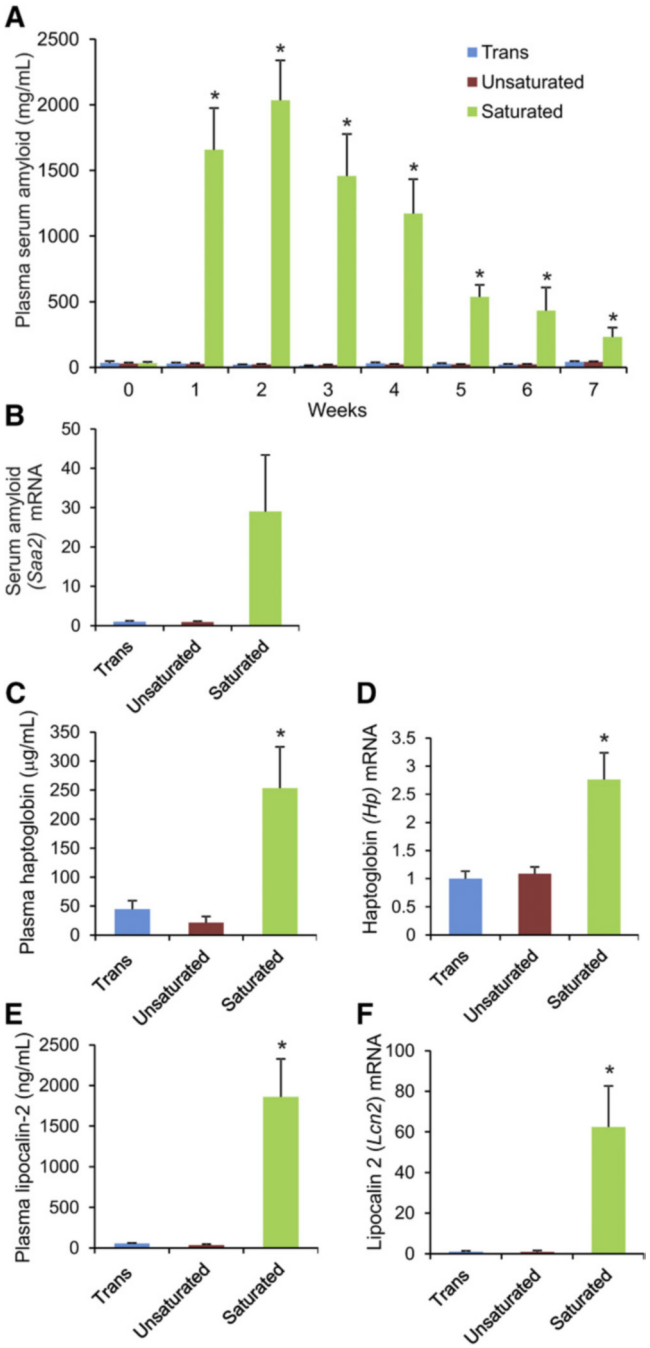


Fig. 2. Feeding *Angptl4*$^{-/-}$ mice a diet rich in saturated, but not *trans*- or *cis*-unsaturated, FAs causes marked elevation of acute phase proteins. *Angptl4*$^{-/-}$ mice were fed the *trans*, unsaturated, or saturated fat diet for 7 weeks. A: Weekly circulating levels of SAA. B: Relative hepatic mRNA level of *Saa2*. C: Plasma levels of haptoglobin. D: Relative hepatic mRNA level of *Hp*. E: Plasma levels of lipocalin-2. F: Relative hepatic mRNA level of *Lcn2*. mRNA expression levels were normalized against *36b4*. Please note that the *Angptl4*$^{-/-}$ mice fed the saturated fat diet were euthanized at different time points due to the implementation of humane endpoints. Error bars represent SEM. Asterisks indicate significantly different relative to *trans* fat group (*$P < 0.05$).

vehicle control. DCFDA oxidation by intracellular ROS generates a fluorescent dicholorofluorescein. Fluorescence signal was measured at excitation/emission wavelengths Ex485/Em538 nm with a Fluoroskan Ascent FL microplate reader. Six replicates were used per individual FA and control treatment.

Immunoblot of unfolded protein response markers

Cell lysates were prepared with RIPA lysis buffer supplemented with protease and phosphatase inhibitors. Protein concentration in lysates was quantified via Bradford assay (Bio-Rad). Samples were boiled for 5 min in SDS-containing buffer before 30 μg of protein lysates were loaded in a mini SDS-PAGE gel. Phos-tag gels were run similarly to regular SDS-PAGE gels complemented with 50 μM $MnCl_2$ (Sigma-Aldrich) and 50 μM Phos-tag (NARD), and by soaking gels for 10 min in 1 mM EDTA before transfer to PVDF membrane, as previously described (31). The primary antibodies that were diluted in 2% BSA in TBST were as follows: HSP90 (#7947; 1:5,000), BiP (#1051; 1:500), α-tubulin (#5286; 1:2,000) from Santa Cruz; inositol requiring kinase 1 (IRE1)α (#3294; 1:2,000), protein kinase RNA-like endoplasmic reticulum (ER) kinase (PERK) (#3192; 1:2,000), cleaved caspase-3 (#9664; 1:1,000) from Cell Signaling; SEL1L (ab78298; 1:2,000), CHOP (ab11419; 1:1,000) from Abcam; XBP1 (#9D11A43; 1:1,000) from BioLegend; HRD1 (kind gift from Dr. Richard Wojcikiewicz; 1:200). The secondary antibodies that were diluted in 5% milk in TBST were anti-rabbit IgG-HRP (Bio-Rad; 1:5,000), anti-mouse IgG-HRP (Bio-Rad; 1:5,000); and anti-goat IgG-HRP (Jackson ImmunoResearch; 1:5,000).

Microarray analysis

Microarray analysis was performed on RAW264.7 macrophages treated with either palmitate, oleate, or elaidate (500 μM) for 6 h. RNA was purified with RNeasy Minikit columns (Qiagen) and analyzed for quality with RNA 6000 Nano chips on the Agilent 2100 bioanalyzer (Agilent Technologies, Amsterdam, The Netherlands). One microgram of RNA was used for cDNA synthesis using the First Strand cDNA synthesis kit (Thermo Scientific). Purified RNA (100 ng) was labeled with the Ambion WT expression kit (Invitrogen) and hybridized to an Affymetrix Mouse Gene 1.1 ST array plate (Affymetrix, Santa Clara, CA). Hybridization, washing, and scanning

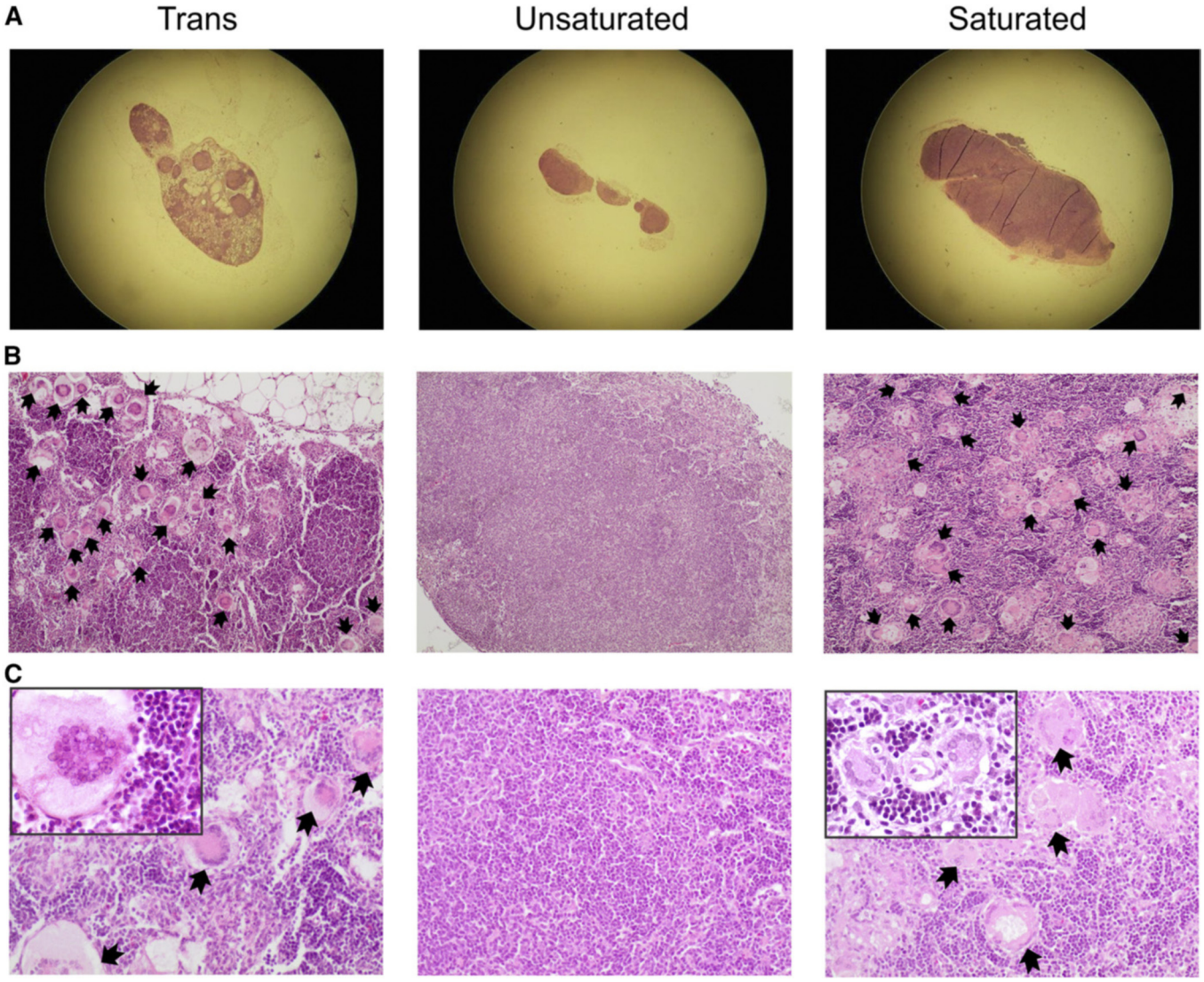


Fig. 3. Feeding *Angptl4*$^{-/-}$ mice a diet rich in *trans* or saturated FAs results in Touton giant cells in MLNs. A: Representative photograph after H&E staining showing enlarged MLN in *Angptl4*$^{-/-}$ mice fed the saturated or *trans* fat diet, but not the *cis* unsaturated fat diet. B: Lower magnification (×100) images showing the relative abundance of Touton giant (foam) cells in the MLN of *Angptl4*$^{-/-}$ mice fed the saturated or *trans* fat diet, but not the *cis* unsaturated fat diet. C: Higher magnification (×200; insert ×400) images of giant cells in MLNs of the *Angptl4*$^{-/-}$ mice fed the *trans* or saturated fat diet. Black arrows indicate giant cells.

were carried out on an Affymetrix GeneTitan platform. Scans of the Affymetrix arrays were processed using packages from the Bioconductor project. Arrays were normalized using the robust multi-array average method (32, 33). Probe sets were defined by assigning probes to unique gene identifiers, e.g., Entrez ID (34). The total gene set (22,135 probe sets) was filtered according to the universal probability code method (score >0.5) (35), resulting in 7,905 probe sets, which were used to generate a scatter plot. An overall heat map was generated using the 500 most variable genes based on calculation of the coefficient of variation. UPC-filtered genes that were induced at least 1.5-fold by palmitate or elaidate relative to oleate were used for Ingenuity pathway analysis (Ingenuity Systems, Redwood City, CA). Microarray data were submitted to the Gene Expression Omnibus (accession number GSE98303).

Lipid analysis

Ceramide and sphingomyelin levels were determined by LC-ESI-MS/MS. RAW 264.7 macrophages from 10 cm cell culture dishes were homogenized in 400 μl of water using the Precellys 24 homogenizator (Peqlab, Erlangen, Germany) at 6,500 rpm for 30 s. To 100 μl of homogenate, 500 μl of methanol, 250 μl of chloroform, and internal standards (127 pmol ceramide 12:0 and 123 pmol sphingomyelin 12:0; both Avanti Polar Lipids, Alabaster, AL) were added. Lipid extraction was performed as previously described (36). Dried lipid extracts were resolved in 300 μl of mobile phase solvent A (see below). LC-MS/MS analysis was performed using a normal phase Nucleosil NH2 column (50 × 2 mm ID, 3 μm particle size, 120 Å pore size; Macherey-Nagel, Dueren, Germany) with detection using a QTRAP 6500 mass spectrometer (SCIEX, Darmstadt, Germany). The LC (1260 Infinity Binary LC System; Agilent, Waldbronn, Germany) was operated at a flow rate of 0.75 ml/min with a mobile phase of acetonitrile/methanol/acetic acid 97:2:1 (v/v/v), with 5 mM ammonium acetate (solvent A) and methanol/acetic acid 99:1 (v/v/v) with 5 mM ammonium acetate (solvent B). LC separation and MS/MS detection were performed as previously described (36). Ceramide and sphingomyelin species were quantified on the basis of calibration curves that were calculated from LC-MS/MS measurements of serially diluted synthetic ceramide and sphingomyelin standards (Avanti Polar Lipids). Linearity and correlation coefficients of the standard curves were obtained via linear regression analysis.

Statistical analysis

Statistical analyses were performed using one-way ANOVA followed by the Tukey HSD test. Data are represented as mean ± SEM (animal studies) or mean ± SD (cell culture studies). $P < 0.05$ was considered statistically significant.

RESULTS

Feeding *Angptl4*$^{-/-}$ mice a diet rich in saturated FAs, but not *trans*- or *cis*-unsaturated FAs, results in peritonitis, chylous ascites, and death

Angptl4$^{-/-}$ mice were randomly assigned to a diet rich in saturated FAs ("Saturated"), a diet rich in *cis*-unsaturated FAs ("Unsaturated"), or a diet rich in *trans*-unsaturated FAs ("Trans"). Different fats were blended to achieve a similar relative content of saturated FAs between the *cis*-unsaturated and the *trans*-unsaturated diets, a similar content of *cis*-unsaturated FAs between the saturated and the *trans*-unsaturated diets, and a complete absence of *trans* FAs in the saturated and *cis*-unsaturated diets. Analysis of the fat composition of the three diets by gas chromatography indicated that approximately 60–65% of the total FA content was constant among the three diets, with the remaining 35–40% of the FAs taken up by saturated FAs, *cis*-unsaturated FAs, or *trans*-unsaturated FAs (**Fig. 1A**). The detailed FA profiles of the three diets are shown in supplemental Table S3. The *Angptl4*$^{-/-}$ mice were fed the diets for 7 weeks. Consistent with our previous studies, *Angptl4*$^{-/-}$ mice fed the saturated fat diet developed anorexia characterized by decreased feed intake (Fig. 1B) and a concomitant steady decline in body weight (Fig. 1C). Six of the eight mice in the saturated fat group became severely ill and showed severe lethargy, reduced responsiveness to stimuli, and abdominal distention. These mice had to be euthanized before the end of the 7 week period, as illustrated by the survival curve (Fig. 1D). Upon euthanasia, *Angptl4*$^{-/-}$ mice fed the saturated fat diet showed an exudate of chylous ascites and fibrinopurulent peritonitis, as previously reported (Fig. 1E). In comparison

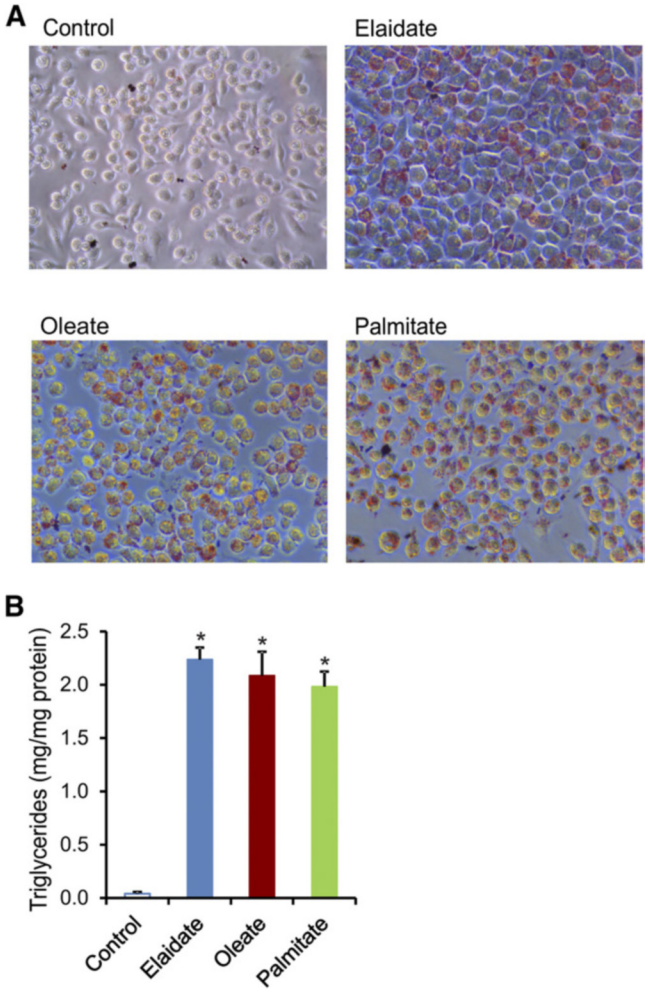


Fig. 4. Similar lipid content in RAW264.7 macrophages treated with different FAs. RAW264.7 macrophages were treated with 500 μM of individual FAs (palmitate, oleate, or elaidate) or vehicle control for 6 h. A: Representative images of oil red O staining of lipid droplets in RAW264.7 macrophages. B: Intracellular triglyceride quantification after FA treatments. Error bars represent SD. Asterisks indicate statistically significant relative to vehicle control (*$P < 0.05$).

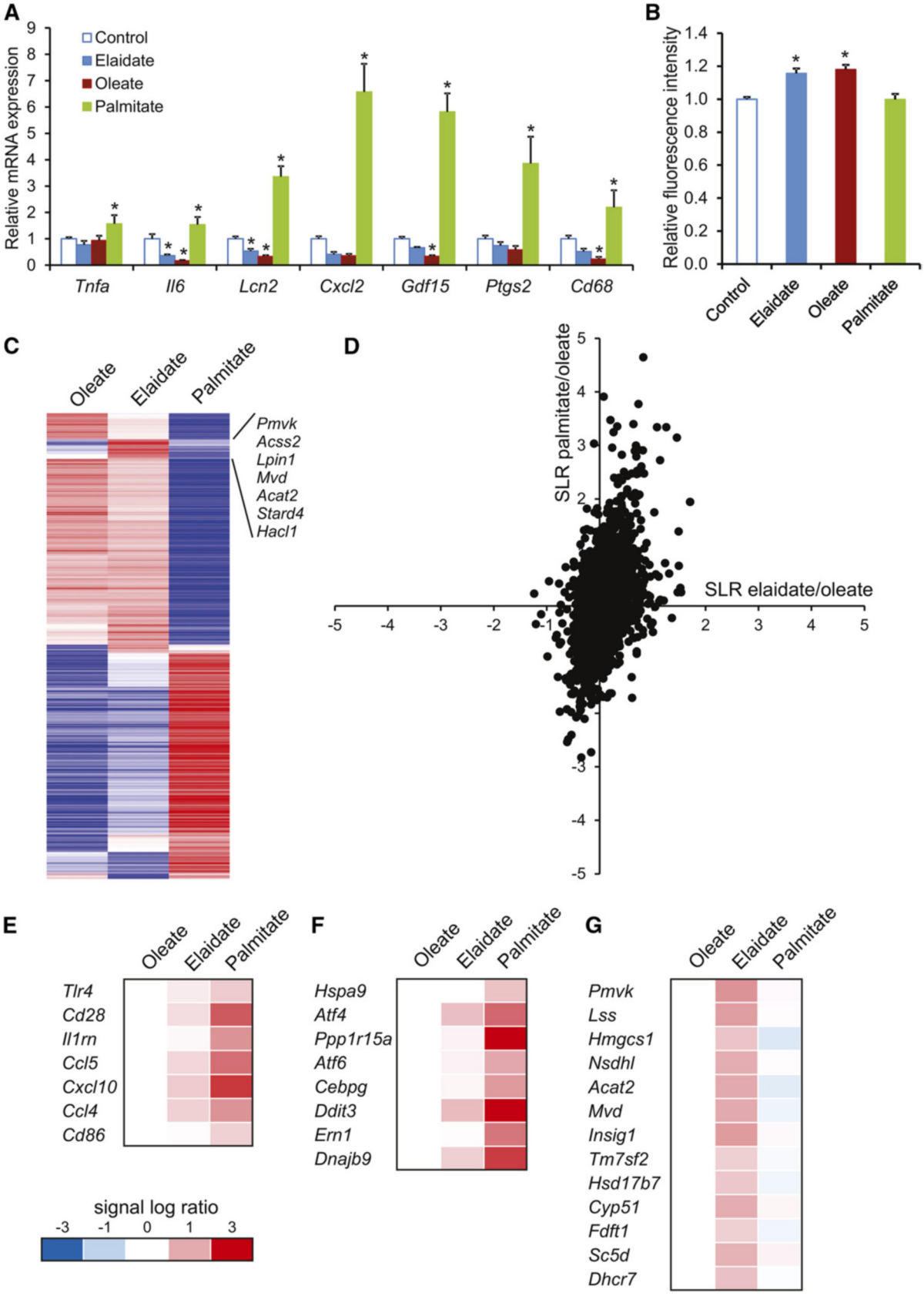


Fig. 5. Differential gene expression profiles in macrophages treated with palmitate, oleate, or elaidate. A: Quantitative PCR expression of selected inflammatory markers in RAW264.7 cells after treatment with 500 μM FAs or vehicle control for 6 h. B: Fluorometric measurement of relative ROS as marker of oxidative stress in RAW264.7 macrophages. C: Heat map of the 500 most variable genes based on the calculation of the coefficient of variation. The cluster of genes deviating in the elaidate-treated cells is indicated. D: Scatter plot of genes that passed the UPC filter (7,905 of the 22,135 probe sets). The signal log ratio for the comparison of palmitate- versus oleate-treated cells is shown along

with earlier experiments, the onset of the development of clinical symptoms in the *Angptl4*$^{-/-}$ mice was more rapid. Remarkably, the observed pathologies were absent both in the *Angptl4*$^{-/-}$ mice fed the *cis*- or *trans*-unsaturated fat diet, even after more prolonged feeding (18 weeks) and in the wild-type mice fed any of the three diets.

After 2 weeks of feeding, prior to becoming visibly ill, plasma glucose levels were significantly lower in the *Angptl4*$^{-/-}$ mice fed the saturated fat diet compared with the other two groups (Fig. 1F). By contrast, plasma insulin levels were the highest in the *Angptl4*$^{-/-}$ mice fed the *trans*-unsaturated fat diet.

Feeding *Angptl4*$^{-/-}$ mice a diet rich in saturated FAs, but not *trans*- or *cis*-unsaturated FAs, causes marked elevation of acute phase proteins

To examine the effect of the three diets on inflammation, we measured plasma levels of the acute phase protein, SAA. Strikingly, whereas *Angptl4*$^{-/-}$ mice fed the saturated fat diet showed a more than 50-fold increase in plasma SAA within 1 week, the mice fed the *trans*- and *cis*-unsaturated fat diet showed no increase at all (**Fig. 2A**). In agreement with these data, liver mRNA levels of *Saa2* at the time of euthanization were significantly elevated in the saturated fat group, but not in the *trans*- or *cis*-unsaturated fat groups (Fig. 2B). Plasma levels of haptoglobin and lipocalin-2, as well as liver mRNA of *Hp* and *Lcn2*, mirrored the SAA data, showing a marked increase in the saturated fat group in comparison to both the *trans*- and *cis*-unsaturated fat groups (Fig. 2C–F). Overall, these data show that feeding *Angptl4*$^{-/-}$ mice a diet rich in *trans*-unsaturated FAs does not lead to chylous ascites and peritonitis, and does not provoke a massive acute phase response, unlike in *Angptl4*$^{-/-}$ mice fed a diet rich in saturated FAs.

Feeding *Angptl4*$^{-/-}$ mice a diet rich in *trans* or saturated FAs stimulates lymphadenopathy characterized by formation of giant cells

We have previously demonstrated that the development of chylous ascites in *Angptl4*$^{-/-}$ mice fed a saturated fat diet is accompanied by mesenteric lymphadenopathy, as shown by enlarged MLNs and the appearance of Touton giant cells (macrophage foam cells). Therefore, in this study, we performed H&E staining on the lymph nodes to examine giant cell formation. In agreement with our earlier studies, lipid-laden giant cells could be observed in the enlarged MLNs of *Angptl4*$^{-/-}$ mice fed the saturated fat diet (six positives out of seven lymph nodes studied). Intriguingly, despite the absence of ascites and any elevation in plasma acute phase proteins, MLNs were enlarged and giant cells were also plentiful in the *Angptl4*$^{-/-}$ mice fed the *trans*-unsaturated fat diet (9 positives out of 13 lymph nodes studied) (**Fig. 3A–**C). No giant cells were observed in the MLN of *Angptl4*$^{-/-}$ mice fed the *cis*-unsaturated fat diet (zero positives out of five lymph nodes studied), nor were they ever observed in wild-type mice. A summary of the observations in the *Angptl4*$^{-/-}$ mice fed the three diets is presented in supplemental Table S4. These data show that mesenteric lymphadenopathy in *Angptl4*$^{-/-}$ mice is uncoupled from the hepatic acute phase response and chylous ascites.

Palmitate, but not elaidate and oleate, stimulates unfolded protein response in cultured macrophages

The experiments in *Angptl4*$^{-/-}$ mice suggest that saturated FAs and *trans*-unsaturated FAs have distinct effects on inflammation, despite both leading to foam cell formation. To study the mechanistic basis for these differences in inflammatory properties, we used RAW264.7 macrophages and incubated these cells either with a saturated FA (palmitate), a *cis*-unsaturated FA (oleate), or a *trans*-unsaturated FA (elaidate). Oil red O staining showed that all three FAs promoted lipid droplet and foam cell formation (**Fig. 4A**). Histological and biochemical analysis did not reveal any differences in lipid accumulation among the three FAs (Fig. 4B). Consistent with the in vivo data, the saturated FA, palmitate, had a pronounced pro-inflammatory effect, as shown by the induction of numerous genes involved in inflammation, including *Ptgs2*, *Cxcl2*, and *Gdf15*, whereas oleate and elaidate caused a modest, yet significant, decrease in inflammatory gene expression (**Fig. 5A**). The differences in inflammatory properties of the FAs could not be explained by differences in activation of oxidative stress, as determined by measuring ROS production (Fig. 5B).

To gain insight into the mechanism(s) underlying the differential properties of palmitate and elaidate, we performed whole genome expression profiling. Visualization of the overall gene expression data by heat map showed that the impact of palmitate on gene expression was very distinct from that of oleate and elaidate (Fig. 5C). In turn, the effects of elaidate and oleate were quite similar with the exception of a cluster of genes involved in lipid and cholesterol synthesis. When related to oleate, palmitate caused much more pronounced changes in gene expression than elaidate, as shown by scatter plot analysis (Fig. 5D). Ingenuity pathway analysis on genes induced by palmitate further corroborated the profound stimulation of inflammatory genes by palmitate. In particular, genes that were part of the pathway, "communication between innate and adaptive immune cells," were highly upregulated by palmitate (rank 6), and to a much lesser extent by elaidate (Fig. 5E). By contrast, the pathway, "superpathway of cholesterol biosynthesis," was specifically induced by elaidate (rank 1) (Fig. 5G). Interestingly, the pathway, "unfolded protein response (UPR)," was highly induced by palmitate (rank 3) when compared with elaidate and oleate (Fig. 5F). Activation of the UPR may provide a mechanistic basis for the pro-inflammatory action of palmitate. UPR maintains cell survival via activation of sensors, such as PERK, activating transcription factor 6 (ATF6), and IRE1, which in turn

the y-axis. The signal log ratio for the comparison of elaidate- versus oleate-treated cells is shown along the x-axis. E–G: Heat maps of pathways that were induced by palmitate: communication between innate and adaptive immune cells (E) and UPR (F), or elaidate: superpathway of cholesterol biosynthesis (G), according to Ingenuity pathway analysis. Asterisks indicate statistically significant relative to vehicle control (*$P < 0.05$).

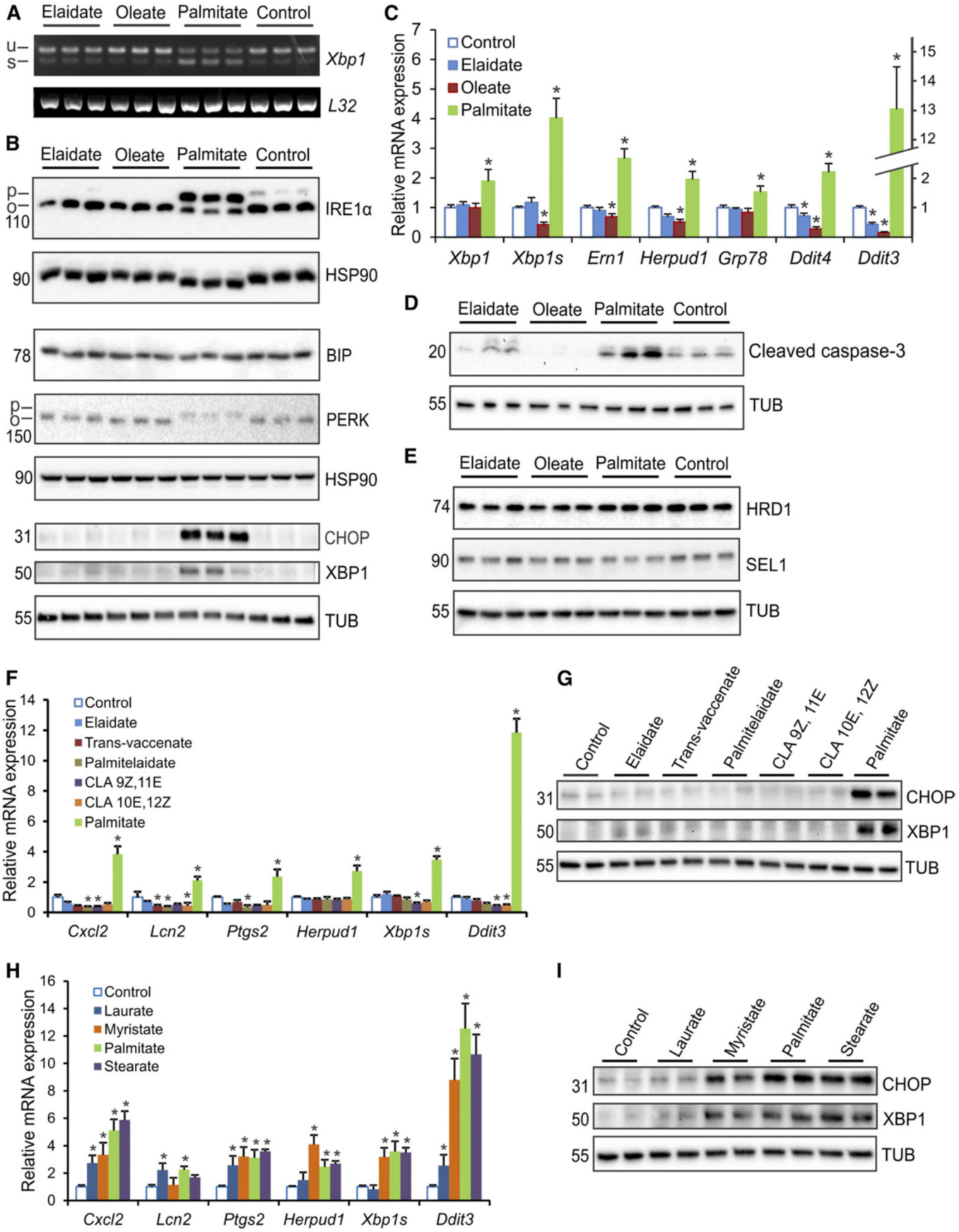


Fig. 6. Palmitate, but not elaidate or oleate, induces UPR and inflammation markers in RAW264.7 macrophages. RAW264.7 macrophages were treated for 6 h with individual FAs (500 μM) as indicated. A: RT-PCR of *Xbp1* processing showing unspliced (u) and spliced (s) *Xbp1* mRNA with L32 as control. B: Immunoblot of UPR downstream effectors and UPR responsive proteins using regular gels (BIP, PERK, CHOP,

triggers the unconventional splicing of *Xbp1* mRNA to generate the transcription factor XBP1 (37–40). Detailed analyses showed that palmitate increased numerous indicators of UPR, including *Xbp1* splicing (**Fig. 6A**), IRE1α phosphorylation, PERK phosphorylation, XBP1 and CHOP protein levels (Fig. 6B), and expression of various ER stress and UPR downstream effector/responsive genes (Fig. 6C), which was not observed for oleate and elaidate. In fact, oleate and elaidate seemed to lead to a mild, but significant, reduction in UPR, as compared with control cells, as indicated by IRE1α phosphorylation, *Ddit3* and *Grp78* mRNA levels, and *Xbp1* alternative splicing. In addition, palmitate induced cleavage of caspase 3, concurrent with upregulation of cell stress markers, suggesting enhanced apoptosis (Fig. 6D). None of these FAs caused the induction of ER-associated degradation proteins, SEL1L and HRD1, under these experimental conditions (Fig. 6E). To verify that the behavior of elaidate was representative of a broader group of *trans*-unsaturated FAs, we studied the effect of *trans*-vaccenate, palmitelaidate, 9Z,11E conjugated linoleate, and 10E,12Z conjugated linoleate in RAW264.7 macrophages. All *trans* FAs led to a similar expression level of a selected group of UPR and inflammation gene markers (Fig. 6F), and all were similarly ineffective toward inducing CHOP and XBP1 protein levels (Fig. 6G), in clear contrast to palmitate. Aside from palmitate, the other saturated FAs, laurate, myristate, and stearate, effectively induced UPR and inflammation marker genes, as well as CHOP and XBP1 protein levels, with a seemingly positive correlation between the magnitude of induction and the length of the FA chain (Fig. 6H, I). These data show that the observed effects of palmitate and elaidate are representative of a larger set of saturated and *trans*-unsaturated FAs, respectively.

Consistent with the results shown above, palmitate markedly raised levels of the lipotoxic mediator, ceramide, as compared with elaidate and oleate, as reflected by the total ceramide levels (**Fig. 7A**) and levels of fatty-acyl subspecies (Fig. 7B). To better delineate the differential lipotoxic effects of saturated and unsaturated FAs, we tested the effect of a number of chemical inhibitors of various pathways of intracellular lipid metabolism, including the ceramide pathway, on palmitate-induced UPR and inflammation in RAW264.7 macrophages. Whereas most compounds showed minimal effects, the CD36 inhibitor, sulfosuccinimidyl oleate, markedly suppressed the induction of *Cxcl2* and *Ddit3* by palmitate, suggesting that cellular FA uptake is necessary for palmitate-induced lipotoxicity (Fig. 7C). By contrast, the sphingosine kinase inhibitor, DMS, and the acyl-CoA synthetase inhibitor, triascin C, markedly augmented the induction of *Cxcl2* and *Ddit3* by palmitate (Fig. 7C). Accordingly, we selected these two compounds to further dissect the differential effects of *trans* and saturated FAs. Remarkably, in the presence of DMS or triascin C, elaidate and oleate lowered expression of UPR and inflammation markers, indicating an anti-lipotoxic action (Fig. 7D). This anti-lipotoxic effect was most pronounced for oleate, but also clearly noticeable for elaidate.

Overall, these data indicate that saturated FAs and *trans* FAs differentially affect UPR and inflammation in cultured macrophages.

DISCUSSION

The work presented in this paper leads to two important conclusions. First, our data show that lipid accumulation and the appearance of giant cells in MLNs (mesenteric lymphadenopathy) in *Angptl4*$^{-/-}$ mice fed a high-fat diet is disconnected from activation of the acute phase response, chylous ascites, and death. Accordingly, the development of mesenteric lymphadenopathy upon ANGPTL4 inactivation may be clinically silent, both in the short and long term, removing part of the concern associated with the use of ANGPTL4-inactivating antibodies as lipid-lowering therapy. Second, we demonstrate that the effects of saturated FAs and *trans* FAs are very distinct, both in vivo and in cultured macrophages. Hence, our data do not support the common notion that *trans* FAs act like saturated FAs.

By virtue of their ability to inhibit LPL and raise circulating triglyceride levels, members of the angiopoietin-like protein family are intensely explored as pharmacological targets for dyslipidemia (41–43). Whereas the targeting of ANGPTL3 has been very successful (44, 45), with strategies to inactivate ANGPTL3 now having moved into clinical trial phase, the targeting of ANGPTL4 has been hampered by the observation that inactivating ANGPTL4 leads to severe clinical problems in mice fed a diet high in saturated fat. Specifically, inactivation of ANGPTL4 causes enhanced lipid uptake into macrophages in MLNs, triggering foam (Touton) cell formation and a massive inflammatory response, which progresses into chylous ascites and ultimately death by peritonitis (17, 46).

Two recent genetic studies generated new interest in ANGPTL4 as a lipid-lowering target by showing that human carriers of an inactivating mutant of ANGPTL4 have a lower risk of coronary artery disease than noncarriers, concomitant with a reduction in serum triglycerides (15, 16). However, one of these studies also found accumulation of lipids in the MLNs in a number of the female monkeys treated with ANGPTL4-inactivating antibodies, copying the symptoms seen in *Angptl4*$^{-/-}$ mice fed a high saturated fat diet (16). These findings raised concern about the possible

and XBP1) and phospho-tag gels (IRE1α). C: Quantitative PCR expression of selected UPR markers. D: Immunoblot of cleaved caspase-3, an indicator of activated cell death by apoptosis. E: Immunoblot of ER-associated protein degradation markers. F: Quantitative PCR expression of selected UPR and inflammation marker genes after treatment with the *trans* FAs, *trans*-vaccenic acid, palmitelaidic acid, CLA 9Z,11E, CLA 10E,12Z, and palmitate. G: Immunoblot of CHOP and XBP1 after treatment with different *trans* FAs and palmitate. H: Quantitative PCR expression of selected UPR and inflammation marker genes after treatment with the saturated FAs, laurate, myristate, palmitate, and stearate. I: Immunoblot of CHOP and XBP1 after treatment with different saturated FAs. mRNA expression was normalized against *36b4*. Error bars represent SD. Asterisks indicate statistically significant relative to vehicle control (*$P < 0.05$).

side-effects of the use of ANGPTL4-inactivating antibodies in humans. In this report, we show that lipid accumulation and the appearance of lipid-laden giant cells in MLNs is uncoupled from the activation of a massive pro-inflammatory response. In particular, we find that despite developing giant cells in their MLNs, *Angptl4*$^{-/-}$ mice fed a diet rich in *trans* FAs do not have elevated plasma serum amyloid and haptoglobin levels, do not develop ascites, and survive, unlike *Angptl4*$^{-/-}$ mice fed a diet rich in saturated FAs. Our findings thus imply that the presence of giant cells in MLNs is nondeleterious and clinically silent, which, together with the reduced risk of coronary artery disease in E40K carriers,

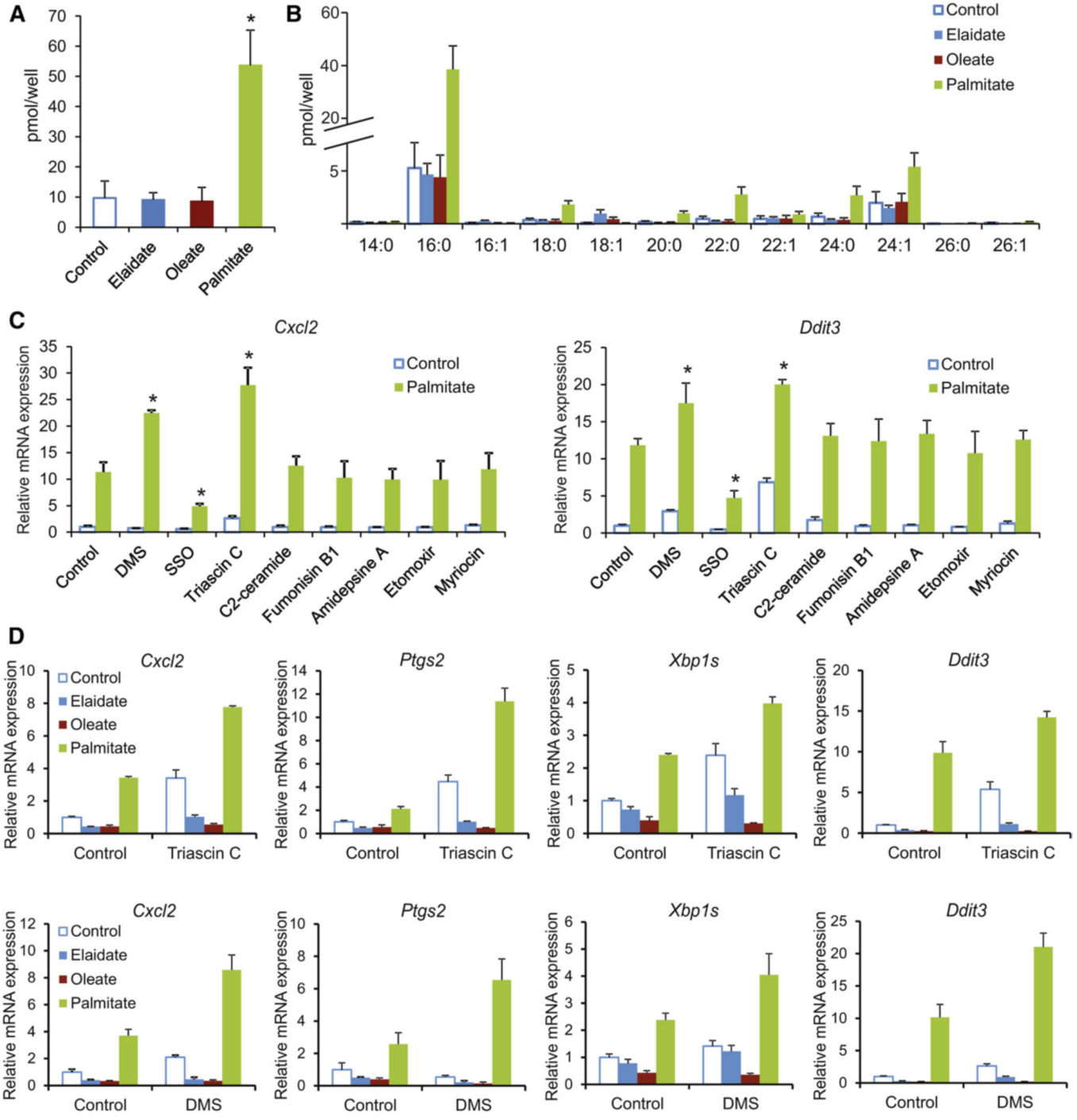


Fig. 7. Anti-lipotoxic effect of oleate and elaidate in RAW264.7 macrophages. RAW264.7 macrophages were treated for 6 h with individual FAs (500 μM) as indicated. Total ceramide levels (A) and levels of ceramide fatty-acyl subspecies (B) after 6 h treatment with elaidate, oleate, palmitate, or vehicle control. C: *Cxcl2* and *Ddit3* expression in RAW264.7 macrophages treated with palmitate or vehicle control and cotreated with the compounds, DMS, sulfosuccinimidyl olate (SSO), triascin C, C2-ceramide, fumonisin B1, amidepsine A, etomoxir, and myriocin. D: Expression of selected UPR and inflammation markers in FA-treated RAW264.7 cells cotreated with either triascin C (top row) or DMS (bottom row). mRNA expression was normalized against *36b4*. Error bars represent SD. Asterisks indicate statistically significant relative to vehicle control (*$P < 0.05$).

suggests that ANGPTL4 may still have promise as a viable therapeutic target for triglyceride lowering and coronary artery disease. To predict future clinical problems, our data also emphasize the need to closely monitor plasma levels of acute phase proteins, both in E40K homozygotes as well as in monkeys and patients that might be treated with ANGPTL4-inactivating antibodies.

Previously, we proposed that elevated LPL activity in MLN macrophages is responsible for the formation of lipid-laden giant cells in *Angptl4*$^{-/-}$ mice fed a high saturated fat diet (17). We hypothesized that the lipid-activated macrophages would release pro-inflammatory cytokines into the portal circulation that activate the hepatic acute phase response. The data presented in this report indicate that the formation of lipid-laden giant cells per se is insufficient to initiate an acute phase response, thus pointing toward an alternative and/or additional mechanism. Based on our in vitro studies, this mechanism requires uptake of FAs, is specifically activated by saturated FAs, and may be linked to the ceramide pathway (see below). Interestingly, *Angptl4*$^{-/-}$ mice do not develop lipid-laden giant cells in MLNs when fed a diet rich in *cis*-unsaturated FAs, even though oleate was equally effective at promoting lipid accumulation in RAW264.7 macrophages. It can be speculated that the development of lipid-laden giant cells in vivo may be dependent on concurrent activation of macrophages or other immune cells, which is triggered by saturated FAs (and *trans*-unsaturated FAs), but not by the more anti-inflammatory *cis*-unsaturated FAs.

Because *trans* and saturated FAs have a similar linear structure, *trans* FAs are claimed to act like saturated FAs. Indeed, nutritional trials have shown that consumption of diets rich in saturated FAs and *trans* FAs both raise LDL-cholesterol levels in humans (23, 47). However, to what extent saturated and *trans* FAs exert the same effects at the cellular level and share the same mechanism of action is unclear. Our results indicate that the biological effects of saturated and *trans* fat in *Angptl4*$^{-/-}$ mice are very different. Whereas feeding a diet rich in saturated fat provoked a pronounced inflammatory response characterized by a huge increase in plasma levels of acute phase proteins, no such response was seen in *Angptl4*$^{-/-}$ mice fed a diet rich in *trans* FAs. Experiments in RAW264.7 macrophages confirmed the distinct biological effects of the saturated FA, palmitate, as compared with the *trans* FA, elaidate. Specifically, whereas palmitate triggered inflammation, UPR, and apoptosis, elaidate induced genes involved in cholesterol synthesis. The properties of palmitate and elaidate were shown to be representative of a whole class of saturated FAs and *trans* FAs, respectively.

The observed lipotoxic properties of palmitate are in line with numerous published studies performed in several cell types where palmitate induced a number of stress-related pathways, such as oxidative stress, inflammation, and UPR (48–52). Several physiological and pathological insults can disturb ER function, leading to the accumulation of unfolded proteins and causing the subsequent activation of UPR. In our studies in RAW264.7 macrophages, we found that palmitate treatment potently activated UPR and inflammatory gene expression. By contrast, elaidate and, especially, oleate suppressed UPR and pro-inflammatory gene expression, which was most evident when baseline levels of UPR and inflammation were raised using DMS or triascin C. These observations are consistent with existing evidence indicating that saturated and *cis*-unsaturated FAs are pro-lipotoxic and anti-lipotoxic, respectively (50, 53–55). Studies have indicated that palmitate may induce ER stress by altering the ER-membrane composition. Indeed, there is evidence that direct sensing of the lipid composition of the ER membrane contributes to the UPR (56, 57). Specifically, it has been suggested that saturated acyl chains are less flexible than unsaturated acyl chains and change the biophysical properties of the membrane to favor dimerization and concomitant activation of IRE1 and PERK (58, 59). If that is true, elaidate would be expected to mimic the properties of palmitate, which was not observed at all. Consistent with our observations, *trans*-unsaturated FAs did not induce ER stress or cytotoxicity in yeast and β cells (60, 61). The modest repressive effect of *trans* FAs on well-established indicators of lipotoxicity, such as UPR and inflammation, is both unexpected and interesting and presents an attractive challenge for further investigation into the potential specific molecular mechanisms behind the purported harmful effects of *trans* fat. Overall, these data underscore the distinct properties of saturated and *trans*-unsaturated FAs.

Treatment of RAW264.7 macrophages with palmitate caused a marked increase in levels of ceramide, which is a known lipotoxic intermediate. However, our studies using a ceramide analog and inhibitors of ceramide synthesis suggest that ceramide itself may not be responsible for the palmitate-induced lipotoxicity. The observed potentiation of the lipotoxic effect of palmitate by DMS has been observed previously (62), and suggests a potential role of sphingosine or sphingosine-1-phosphate. Besides DMS, the acyl-CoA synthesis inhibitor, triascin C, also potentiated palmitate-induced lipotoxicity. This result is in line with a similar study in mouse peritoneal macrophages treated with stearate (63) and suggests that lipotoxicity is mediated by free palmitate/stearate. Based on our experiments, it is not possible to attribute the lipotoxic effects of palmitate to a single well-defined mechanism.

In conclusion, our data indicate that the presence of lipid-laden giant cells in MLNs is uncoupled from the acute phase response and chylous ascites. The probable nondeleterious effect of foam cells in MLNs of ANGPTL4-deficient mice suggests that ANGPTL4 should not be fully dismissed as a target for correcting dyslipidemia and atherosclerosis in humans. Finally, our in vitro and in vivo data strongly indicate that *trans* and saturated FAs have distinct biological effects, with the *trans* FAs leaning much more toward *cis*-unsaturated FAs than toward saturated FAs.

REFERENCES

1. Wang, H., and R. H. Eckel. 2009. Lipoprotein lipase: from gene to obesity. *Am. J. Physiol. Endocrinol. Metab.* **297:** E271–E288.
2. Myocardial Infarction Genetics and CARDIoGRAM Exome Consortia. 2016. Coding variation in ANGPTL4, LPL, and SVEP1 and the risk of coronary disease. *N. Engl. J. Med.* **374:** 1134–1144.

3. Fong, L. G., S. G. Young, A. P. Beigneux, A. Bensadoun, M. Oberer, H. Jiang, and M. Ploug. 2016. GPIHBP1 and plasma triglyceride metabolism. *Trends Endocrinol. Metab.* **27:** 455–469.
4. Beigneux, A. P., R. Franssen, A. Bensadoun, P. Gin, K. Melford, J. Peter, R. L. Walzem, M. M. Weinstein, B. S. J. Davies, J. A. Kuivenhoven, et al. 2009. Chylomicronemia with a mutant GPIHBP1 (Q115P) that cannot bind lipoprotein lipase. *Arterioscler. Thromb. Vasc. Biol.* **29:** 956–962.
5. Beigneux, A. P., B. S. J. Davies, P. Gin, M. M. Weinstein, E. Farber, X. Qiao, F. Peale, S. Bunting, R. L. Walzem, J. S. Wong, et al. 2007. Glycosylphosphatidylinositol-anchored high-density lipoprotein-binding protein 1 plays a critical role in the lipolytic processing of chylomicrons. *Cell Metab.* **5:** 279–291.
6. Dijk, W., and S. Kersten. 2014. Regulation of lipoprotein lipase by Angptl4. *Trends Endocrinol. Metab.* **25:** 146–155.
7. Catoire, M., S. Alex, N. Paraskevopulos, F. Mattijssen, I. Evers-van Gogh, G. Schaart, J. Jeppesen, A. Kneppers, M. Mensink, P. J. Voshol, et al. 2014. Fatty acid-inducible ANGPTL4 governs lipid metabolic response to exercise. *Proc. Natl. Acad. Sci. USA.* **111:** E1043–E1052.
8. Kersten, S., S. Mandard, N. S. Tan, P. Escher, D. Metzger, P. Chambon, F. J. Gonzalez, B. Desvergne, and W. Wahli. 2000. Characterization of the fasting-induced adipose factor FIAF, a novel peroxisome proliferator-activated receptor target gene. *J. Biol. Chem.* **275:** 28488–28493.
9. Yoon, J. C., T. W. Chickering, E. D. Rosen, B. Dussault, Y. Qin, A. Soukas, J. M. Friedman, W. E. Holmes, and B. M. Spiegelman. 2000. Peroxisome proliferator-activated receptor gamma target gene encoding a novel angiopoietin-related protein associated with adipose differentiation. *Mol. Cell. Biol.* **20:** 5343–5349.
10. Dijk, W., A. P. Beigneux, M. Larsson, A. Bensadoun, S. G. Young, and S. Kersten. 2016. Angiopoietin-like 4 (ANGPTL4) promotes intracellular degradation of lipoprotein lipase in adipocytes. *J. Lipid Res.* **57:** 1670–1683.
11. Sukonina, V., A. Lookene, T. Olivecrona, and G. Olivecrona. 2006. Angiopoietin-like protein 4 converts lipoprotein lipase to inactive monomers and modulates lipase activity in adipose tissue. *Proc. Natl. Acad. Sci. USA.* **103:** 17450–17455.
12. Mandard, S., F. Zandbergen, E. Van Straten, W. Wahli, F. Kuipers, M. Müller, and S. Kersten. 2006. The fasting-induced adipose factor/angiopoietin-like protein 4 is physically associated with lipoproteins and governs plasma lipid levels and adiposity. *J. Biol. Chem.* **281:** 934–944.
13. Köster, A., Y. B. Chao, M. Mosior, A. Ford, P. A. Gonzalez-DeWhitt, J. E. Hale, D. Li, Y. Qiu, C. C. Fraser, D. D. Yang, et al. 2005. Transgenic angiopoietin-like (Angptl)4 overexpression and targeted disruption of Angptl4 and Angptl3: regulation of triglyceride metabolism. *Endocrinology.* **146:** 4943–4950.
14. Sonnenburg, W. K., D. Yu, E-C. Lee, W. Xiong, G. Gololobov, B. Key, J. Gay, N. Wilganowski, Y. Hu, S. Zhao, et al. 2009. GPIHBP1 stabilizes lipoprotein lipase and prevents its inhibition by angiopoietin-like 3 and angiopoietin-like 4. *J. Lipid Res.* **50:** 2421–2429.
15. Abid, K., T. Trimeche, D. Mili, M. A. Msolli, I. Trabelsi, S. Nouira, and A. Kenani. 2016. ANGPTL4 variants E40K and T266M are associated with lower fasting triglyceride levels and predicts cardiovascular disease risk in type 2 diabetic Tunisian population. *Lipids Health Dis.* **15:** 63.
16. Dewey, F. E., V. Gusarova, C. O'Dushlaine, O. Gottesman, J. Trejos, C. Hunt, C. V. Van Hout, L. Habegger, D. Buckler, K. M. Lai, et al. 2016. Inactivating variants in ANGPTL4 and risk of coronary artery disease. *N. Engl. J. Med.* **374:** 1123–1133.
17. Lichtenstein, L., F. Mattijssen, N. J. de Wit, A. Georgiadi, G. J. Hooiveld, R. van der Meer, Y. He, L. Qi, A. Köster, J. T. Tamsma, et al. 2010. Angptl4 protects against severe proinflammatory effects of saturated fat by inhibiting fatty acid uptake into mesenteric lymph node macrophages. *Cell Metab.* **12:** 580–592.
18. Bassett, C. M. C., A. L. Edel, A. F. Patenaude, R. S. McCullough, D. P. Blackwood, P. Y. Chouinard, P. Paquin, B. Lamarche, and G. N. Pierce. 2010. Dietary vaccenic acid has antiatherogenic effects in LDLr-/- mice. *J. Nutr.* **140:** 18–24.
19. Stender, S., A. Astrup, and J. Dyerberg. 2008. Ruminant and industrially produced trans fatty acids: health aspects. *Food Nutr. Res.* **52:** 1–8.
20. Mozaffarian, D., M. B. Katan, A. Ascherio, M. J. Stampfer, and W. C. Willett. 2006. Trans fatty acids and cardiovascular disease. *N. Engl. J. Med.* **354:** 1601–1613.
21. Ganguly, R., and G. N. Pierce. 2012. Trans fat involvement in cardiovascular disease. *Mol. Nutr. Food Res.* **56:** 1090–1096.
22. Ginter, E., and V. Simko. 2016. New data on harmful effects of trans-fatty acids. *Bratisl. Lek. Listy.* **117:** 251–253.
23. de Souza, R. J., A. Mente, A. Maroleanu, A. I. Cozma, V. Ha, T. Kishibe, E. Uleryk, P. Budylowski, H. Schünemann, J. Beyene, et al. 2015. Intake of saturated and trans unsaturated fatty acids and risk of all cause mortality, cardiovascular disease, and type 2 diabetes: systematic review and meta-analysis of observational studies. *BMJ.* **351:** h3978.
24. Willett, W. C., M. J. Stampfer, J. E. Manson, G. A. Colditz, F. E. Speizer, B. A. Rosner, L. A. Sampson, and C. H. Hennekens. 1993. Intake of trans fatty acids and risk of coronary heart disease among women. *Lancet.* **341:** 581–585.
25. Eckel, R. H., S. Borra, A. H. Lichtenstein, and S. Y. Yin-Piazza. 2007. Understanding the complexity of trans fatty acid reduction in the American diet: American heart association trans fat conference 2006: report of the trans fat conference planning group. *Circulation.* **115:** 2231–2246.
26. Kaur, G., D. Cameron-Smith, and A. J. Sinclair. 2012. Are trans fats a problem in Australia? *Med. J. Aust.* **196:** 666–667.
27. L'Abbé, M. R., S. Stender, C. M. Skeaff, Ghafoorunissa, and M. Tavella. 2009. Approaches to removing trans fats from the food supply in industrialized and developing countries. *Eur. J. Clin. Nutr.* **63:** S50–S67.
28. Stender, S., J. Dyerberg, and A. Astrup. 2006. Consumer protection through a legislative ban on industrially produced trans fatty acids in foods in Denmark. *Scand. J. Food Nutr.* **50:** 155–160.
29. Pérez-Farinós, N., M. Á. Dal Re Saavedra, C. Villar Villalba, and T. Robledo de Dios. 2016. Trans-fatty acid content of food products in Spain in 2015. *Gac. Sanit.* **30:** 379–382.
30. Folch, J., M. Lees, and G. H. Sloane Stanley. 1957. A simple method for the isolation and purification of total lipides from animal tissues. *J. Biol. Chem.* **226:** 497–509.
31. Yang, L., Z. Xue, Y. He, S. Sun, H. Chen, and L. Qi. 2010. A Phos-tag-based approach reveals the extent of physiological endoplasmic reticulum stress. *PLoS One.* **5:** e11621.
32. Irizarry, R. A., B. Hobbs, F. Collin, Y. D. Beazer-Barclay, K. J. Antonellis, U. Scherf, and T. P. Speed. 2003. Exploration, normalization, and summaries of high density oligonucleotide array probe level data. *Biostatistics.* **4:** 249–264.
33. Bolstad, B. M., R. A. Irizarry, M. Astrand, and T. P. Speed. 2003. A comparison of normalization methods for high density oligonucleotide array data based on variance and bias. *Bioinformatics.* **19:** 185–193.
34. Dai, M., P. Wang, A. D. Boyd, G. Kostov, B. Athey, E. G. Jones, W. E. Bunney, R. M. Myers, T. P. Speed, H. Akil, et al. 2005. Evolving gene/transcript definitions significantly alter the interpretation of GeneChip data. *Nucleic Acids Res.* **33:** e175.
35. Piccolo, S. R., M. R. Withers, O. E. Francis, A. H. Bild, and W. E. Johnson. 2013. Multiplatform single-sample estimates of transcriptional activation. *Proc. Natl. Acad. Sci. USA.* **110:** 17778–17783.
36. Schwamb, J., V. Feldhaus, M. Baumann, M. Patz, S. Brodesser, R. Brinker, J. Claasen, C. P. Pallasch, M. Hallek, C. M. Wendtner, et al. 2012. B-cell receptor triggers drug sensitivity of primary CLL cells by controlling glucosylation of ceramides. *Blood.* **120:** 3978–3985.
37. Han, J., and R. J. Kaufman. 2016. The role of ER stress in lipid metabolism and lipotoxicity. *J. Lipid Res.* **57:** 1329–1338.
38. Bensellam, M., E. L. Maxwell, J. Y. Chan, J. Luzuriaga, P. K. West, J-C. Jonas, J. E. Gunton, and D. R. Laybutt. 2016. Hypoxia reduces ER-to-Golgi protein trafficking and increases cell death by inhibiting the adaptive unfolded protein response in mouse beta cells. *Diabetologia.* **59:** 1492–1502.
39. Chen, Y., and F. Brandizzi. 2013. IRE1: ER stress sensor and cell fate executor. *Trends Cell Biol.* **23:** 547–555.
40. Gupta, S., A. Deepti, S. Deegan, F. Lisbona, C. Hetz, and A. Samali. 2010. HSP72 protects cells from ER stress-induced apoptosis via enhancement of IRE1α-xbp1 signaling through a physical interaction. *PLoS Biol.* **8:** e1000410.
41. Fu, Z., A. B. Abou-Samra, and R. Zhang. 2015. A lipasin/Angptl8 monoclonal antibody lowers mouse serum triglycerides involving increased postprandial activity of the cardiac lipoprotein lipase. *Sci. Rep.* **5:** 18502.
42. Li, Y., and C. Teng. 2014. Angiopoietin-like proteins 3, 4 and 8: regulating lipid metabolism and providing new hope for metabolic syndrome. *J. Drug Target.* **22:** 679–687.
43. Zhang, R. 2016. The ANGPTL3-4-8 model, a molecular mechanism for triglyceride trafficking. *Open Biol.* **6:** 150272.

44. Gusarova, V., C. a. Alexa, Y. Wang, A. Rafique, J. H. Kim, D. Buckler, I. J. Mintah, L. M. Shihanian, J. C. Cohen, H. H. Hobbs, et al. 2015. ANGPTL3 blockade with a human monoclonal antibody reduces plasma lipids in dyslipidemic mice and monkeys. *J. Lipid Res.* **56:** 1308–1317.
45. Wang, Y., V. Gusarova, S. Banfi, J. Gromada, J. C. Cohen, and H. H. Hobbs. 2015. Inactivation of ANGPTL3 reduces hepatic VLDL-triglyceride secretion. *J. Lipid Res.* **56:** 1296–1307.
46. Desai, U., E. C. Lee, K. Chung, C. Gao, J. Gay, B. Key, G. Hansen, D. Machajewski, K. A. Platt, A. T. Sands, et al. 2007. Lipid-lowering effects of anti-angiopoietin-like 4 antibody recapitulate the lipid phenotype found in angiopoietin-like 4 knockout mice. *Proc. Natl. Acad. Sci. USA.* **104:** 11766–11771.
47. Siri-Tarino, P. W., Q. Sun, F. B. Hu, and R. M. Krauss. 2010. Saturated fatty acids and risk of coronary heart disease: modulation by replacement nutrients. *Curr. Atheroscler. Rep.* **12:** 384–390.
48. Cao, J., D-L. Dai, L. Yao, H-H. Yu, B. Ning, Q. Zhang, J. Chen, W-H. Cheng, W. Shen, and Z-X. Yang. 2012. Saturated fatty acid induction of endoplasmic reticulum stress and apoptosis in human liver cells via the PERK/ATF4/CHOP signaling pathway. *Mol. Cell. Biochem.* **364:** 115–129.
49. Egnatchik, R. A., A. K. Leamy, Y. Noguchi, M. Shiota, and J. D. Young. 2014. Palmitate-induced activation of mitochondrial metabolism promotes oxidative stress and apoptosis in H4IIEC3 rat hepatocytes. *Metabolism.* **63:** 283–295.
50. Schilling, J. D., H. M. Machkovech, L. He, R. Sidhu, H. Fujiwara, K. Weber, D. S. Ory, and J. E. Schaffer. 2013. Palmitate and lipopolysaccharide trigger synergistic ceramide production in primary macrophages. *J. Biol. Chem.* **288:** 2923–2932.
51. Leamy, A. K., C. M. Hasenour, R. A. Egnatchik, I. A. Trenary, C. H. Yao, G. J. Patti, M. Shiota, and J. D. Young. 2016. Knockdown of triglyceride synthesis does not enhance palmitate lipotoxicity or prevent oleate-mediated rescue in rat hepatocytes. *Biochim. Biophys. Acta.* **1861:** 1005–1014.
52. Robblee, M. M., C. C. Kim, J. Porter Abate, M. Valdearcos, K. L. Sandlund, M. K. Shenoy, R. Volmer, T. Iwawaki, and S. K. Koliwad. 2016. Saturated fatty acids engage an IRE1α-dependent pathway to activate the NLRP3 inflammasome in myeloid cells. *Cell Rep.* **14:** 2611–2623.
53. Dumas, J. A., J. Y. Bunn, J. Nickerson, K. I. Crain, D. B. Ebenstein, E. K. Tarleton, J. Makarewicz, M. E. Poynter, and C. L. Kien. 2016. Dietary saturated fat and monounsaturated fat have reversible effects on brain function and the secretion of pro-inflammatory cytokines in young women. *Metabolism.* **65:** 1582–1588.
54. L'homme, L., N. Esser, L. Riva, A. Scheen, N. Paquot, J. Piette, and S. Legrand-Poels. 2013. Unsaturated fatty acids prevent activation of NLRP3 inflammasome in human monocytes/macrophages. *J. Lipid Res.* **54:** 2998–3008.
55. Kennedy, A., K. Martinez, C-C. Chuang, K. LaPoint, and M. McIntosh. 2009. Saturated fatty acid-mediated inflammation and insulin resistance in adipose tissue: mechanisms of action and implications. *J. Nutr.* **139:** 1–4.
56. Borradaile, N. M., X. Han, J. D. Harp, S. E. Gale, D. S. Ory, and J. E. Schaffer. 2006. Disruption of endoplasmic reticulum structure and integrity in lipotoxic cell death. *J. Lipid Res.* **47:** 2726–2737.
57. Leamy, A. K., R. A. Egnatchik, M. Shiota, P. T. Ivanova, D. S. Myers, H. A. Brown, and J. D. Young. 2014. Enhanced synthesis of saturated phospholipids is associated with ER stress and lipotoxicity in palmitate treated hepatic cells. *J. Lipid Res.* **55:** 1478–1488.
58. Volmer, R., K. van der Ploeg, and D. Ron. 2013. Membrane lipid saturation activates endoplasmic reticulum unfolded protein response transducers through their transmembrane domains. *Proc. Natl. Acad. Sci. USA.* **110:** 4628–4633.
59. Kitai, Y., H. Ariyama, N. Kono, D. Oikawa, T. Iwawaki, and H. Arai. 2013. Membrane lipid saturation activates IRE1α without inducing clustering. *Genes Cells.* **18:** 798–809.
60. Deguil, J., L. Pineau, E. C. Rowland Snyder, S. Dupont, L. Beney, A. Gil, G. Frapper, and T. Ferreira. 2011. Modulation of lipid-induced ER stress by fatty acid shape. *Traffic.* **12:** 349–362.
61. Dhayal, S., H. J. Welters, and N. G. Morgan. 2008. Structural requirements for the cytoprotective actions of mono-unsaturated fatty acids in the pancreatic beta-cell line, BRIN-BD11. *Br. J. Pharmacol.* **153:** 1718–1727.
62. Hamada, Y., H. Nagasaki, A. Fujiya, Y. Seino, Q. L. Shang, T. Suzuki, H. Hashimoto, and Y. Oiso. 2014. Involvement of de novo ceramide synthesis in pro-inflammatory adipokine secretion and adipocyte-macrophage interaction. *J. Nutr. Biochem.* **25:** 1309–1316.
63. Anderson, E. K., A. A. Hill, and A. H. Hasty. 2012. Stearic acid accumulation in macrophages induces toll-like receptor 4/2-independent inflammation leading to endoplasmic reticulum stress-mediated apoptosis. *Arterioscler. Thromb. Vasc. Biol.* **32:** 1687–1695.